Inorganic Chemistry

Article

pubs.acs.org/IC

Ca K-Edge XAS as a Probe of Calcium Centers in Complex Systems

Vlad Martin-Diaconescu,[†] Marcello Gennari,[‡] Bertrand Gerey,[‡] Emily Tsui,[§] Jacob Kanady,[§] Rosalie Tran,[∥] Jacques Pécaut,[⊥] Dimitrios Maganas,[†] Vera Krewald,[†] Eric Gouré,[‡] Carole Duboc,[‡] Junko Yano,[∥] Theodor Agapie,[§] Marie-Noelle Collomb,[‡] and Serena DeBeer*[,†,#]

[†]Max Planck Institute for Chemical Energy Conversion, Stiftstrasse 34-36, D-45470 Mülheim an der Ruhr, Germany

[‡]Univ. Grenoble Alpes, DCM and CNRS, DCM, F-38000 Grenoble, France

[§]California Institute of Technology, Department of Chemistry, Pasadena, California 91125, United States

[∥]Lawrence Berkeley National Laboratory − Physical Biosciences Division, Berkeley, California 94720, United States

[⊥]Laboratoire de Reconnaissance Ionique et Chimie de Coordination (LCIB, SCIB, INAC, CEA Grenoble), 38054 Grenoble Cedex 9, France

[#]Department of Chemistry and Chemical Biology, Cornell University, Ithaca, New York 14853, United States

Supporting Information

ABSTRACT: Herein, Ca K-edge X-ray absorption spectroscopy (XAS) is developed as a means to characterize the local environment of calcium centers. The spectra for six, seven, and eight coordinate inorganic and molecular calcium complexes were analyzed and determined to be primarily influenced by the coordination environment and site symmetry at the calcium center. The experimental results are closely correlated to time-dependent density functional theory (TD-DFT) calculations of the XAS spectra. The applicability of this methodology to complex systems was investigated using structural mimics of the oxygen-evolving complex (OEC) of PSII. It was found that Ca K-edge XAS is a sensitive probe for structural changes occurring in the cubane heterometallic cluster due to Mn oxidation. Future applications to the OEC are discussed.

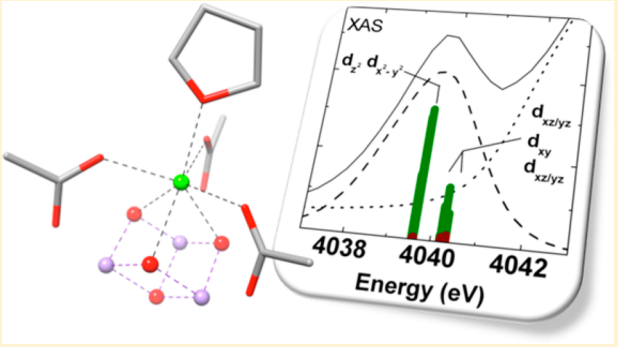

INTRODUCTION

Calcium serves essential functions in numerous biological and chemical processes. In nature, calcium is a regulator of intracellular processes,[1−4] activates proteases,[5−7] and is essential for photosystem II (PSII) maturation[8] and catalytic activity.[9−11] In industrial processes, calcium oxide plays a role as a heterogeneous catalyst in transesterification reactions, offering the promise of environmentally sustainable exploitation of biofuels.[12−14] Calcium also plays an important role as a promoter in transition metal-mediated heterogeneous processes.[15] Additionally, the use of calcium compounds in homogeneous catalysis has received increasing attention, with applications in polymerization catalysis, hydroamination, and hydrosilylation.[16−20] The earth abundance of calcium, as well as its biocompatibility, provides motivation for further development of Ca-based catalysts.

In order to understand the transformations that occur at the calcium site, in both chemical and biological processes, one would like to selectively probe the calcium coordination environment. In this sense, Ca K-edge X-ray absorption spectroscopy (XAS) is an ideal tool. Ca K-edge XAS results from the excitation of Ca 1s electrons to empty molecular orbitals localized on the calcium atom. As such, Ca XAS should provide a sensitive probe of the Ca coordination environment. However, to our knowledge, a thorough investigation of Ca K-edge XAS has not yet been made. Previous Ca K-edge XAS studies have generally used a fingerprinting approach, and only limited studies exist in which Ca K-edge data have been correlated to theory.[21−27] The majority of the quantitative information that has been obtained from Ca XAS data has largely relied on the extraction of metal−ligand bond distances and coordination numbers from the EXAFS region.[21,26−31] However, due to the large inherent error in establishing coordination numbers from EXAFS (~25%), the ability to determine accurate coordination numbers from EXAFS alone is limited. However, previous studies have successfully coupled K-edge analysis with EXAFS analysis to describe previously uncharacterized metal centers in complex systems such as proteins.[32−38] Therefore, the development of Ca K-edge XAS should significantly aid in the characterization of Ca centers. In principle, the information content of Ca XAS may be greatly enhanced through a quantitative analysis of the pre-edge

Received: August 15, 2014
Published: December 10, 2014

   dx.doi.org/10.1021/ic501991e | Inorg. Chem. 2015, 54, 1283−1292

Table 1. List of Compounds and Their Properties

compound	label	coordination	local symmetry[a]	experimental		calculated	
				energy (eV)	intensity ($\times 10^2$)	energy (eV)	intensity ($\times 10^6$)
CaO	**6**[a]	6	O_h	4039.26(5)	3.8(9)	3989.45	6.06
				4040.62(2)	2.5(6)	3990.59	4.94
CaCO3	**6**[b]	6	O_h/D_{4h}	4039.78(3)	3.8(3)	3989.45	6.97
				4040.78(3)	4.4(3)	3990.56	4.86
$Ca(OH)_2$	**6**[c]	6	O_h/D_{4h}	4039.50(5)	3.8(7)	3989.35	7.00
				4040.65(8)	2.5(1)	3990.62	5.16
$\{[LMn^{II}Mn^{III}{}_2O(OAc)_3]_2Ca\}^{+2}$	**6**[d]	6	O_h/D_{4h}	4039.62(25)	1.1(6)	3989.42	2.16
				4040.28(26)	1.1(8)	3990.43	1.56
$[LMn^{IV}Mn^{III}{}_2CaO_2(OAc)_2(DME)(OTf)]^{+2}$	7^{NCox}	7	C_{2V}/C_{3V}	4040.13(8)	20.2(30)	3989.83	44.23
$[LMn^{III}CaO_2(OAc)_2(DME)(OTf)]^{+1}$	7^{NCred}	7	C_{2V}/C_{3V}	4040.20(8)	23.0(34)	3989.93	52.85
$LMn^{IV}{}_3CaO_4(OAc)_3(THF)$	7^{e}	7	C_{3V}	4039.77(5)	42.0(21)	3989.59	126.84
$LMn^{IV}{}_3CaO_4(OAc)_3(DMF)$	7^{CUBox}	7	C_{3V}	4039.71(1)	41.5(5)	3989.50	124.25
$[LMn^{IV}{}_2Mn^{III}CaO_4(OAc)_3(DMF)]^-$	7^{CUBred}	7		4039.73(1)	34.9(9)		
$[Ca(Htpaa)(H_2O)]$	**8**[f]	8	D_{2d}	4040.08(2)	23.1(7)	3989.95	69.40
$[Ca(dpaea)(H_2O)(MeOH)]_2$	**8**[g]	8	D_{2d}	4040.23(2)	19.0(10)	3989.89	52.94
$[Mn_2(tpaa)_2Ca_2(H_2O)_{12}]$	**8**[h]	8	D_{4d}/D_{2d}	4040.36(10)	15.0(20)	3989.98	19.60
$\{[Ca_2(bzida)_2(H_2O)_6]\}_n$	**8**[i]	8	D_{4d}/D_{2d}	4040.15(1)	14.7(2)	3990.00	29.30

[a]Approximate symmetry at the calcium center.

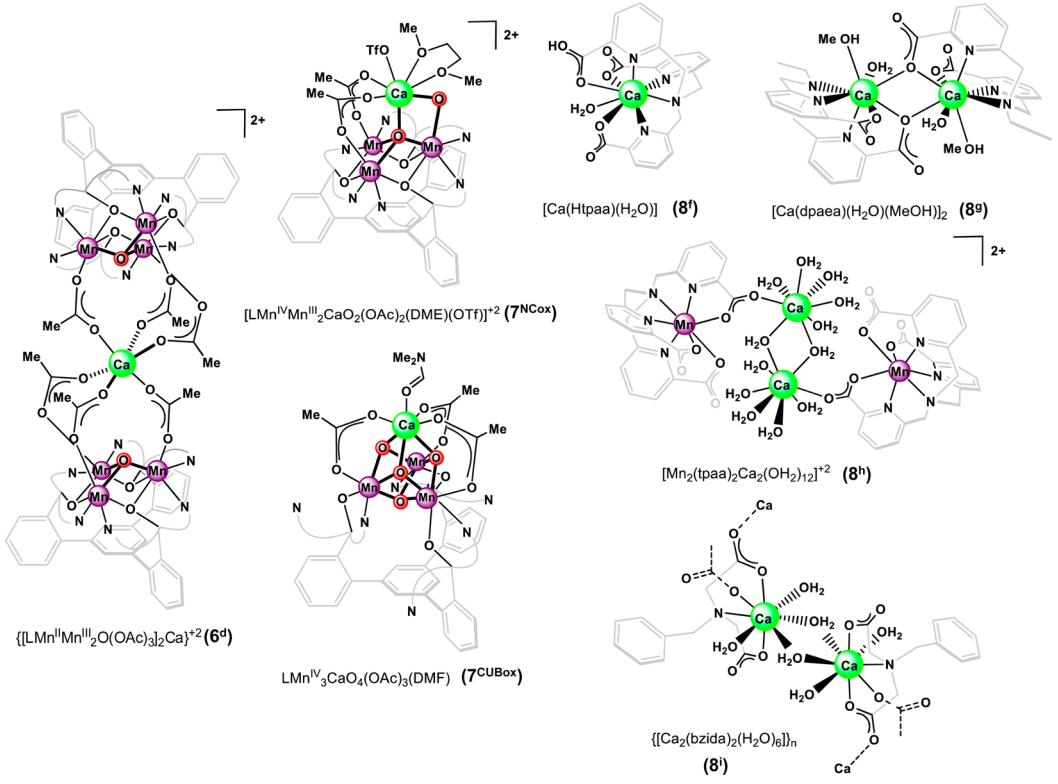

Figure 1. Structures of molecular complexes. Representative structures for the seven coordinate "noncubane" (7^{NCox} and 7^{NCred}) and "cubane-like" complexes (7^{CUBox}, 7^{CUBred}, 7^{e}) are shown. In the 7^{e} complex, a tetrahydrofuran ligand replaces the dimethylformamide seen in the 7^{CUB} series.

spectral region, in a manner analogous to previous studies on first row transition metals.[39−50]

Herein, we systematically investigate the information content of Ca K-pre-edge XAS and extend these studies to complex heterometallic MnCa clusters with relevance to the oxygen-evolving complex (OEC) of PSII, which consists of a Mn_4O_5Ca cluster with a "distorted chair" conformation formed from an oxo-bridged "cubane-like" Mn_3O_4Ca core connected to a "dangling" Mn by oxo-bridges.[51] Ca K-edge XAS data were obtained for a series of six, seven, and eight coordinate calcium compounds (Table 1 and Figure 1), including molecular and inorganic lattice species, in order to establish the experimental changes that occur in the Ca pre-edge XAS region upon altering the coordination environment of the Ca^{2+} ion. Experimental intensity and energy correlations are observed, which can be interpreted within a simple ligand field picture. Further, we apply a TD-DFT protocol, which allows for the calculation of XAS pre-edges for both molecular and inorganic lattice systems, with excellent reliability.

dx.doi.org/10.1021/ic501991e | Inorg. Chem. 2015, 54, 1283−1292

Having established the correlation between experiment and theory, we then further explore the applicability of this approach to understanding the changes that occur at the Ca center in complex heterometallic systems. In particular, structural information is extracted from the changes in the Ca K-pre-edge associated with a one electron reduction of the cubane Mn_3O_4Ca cluster (Figure 1), which serves as a structural reference point of the Mn_4O_5Ca cluster in the OEC. As calcium is often suggested to play a mechanistic role in water oxidation, the changes that occur at the Ca site during the catalytic cycle are of fundamental interest. Our results show that direct correlation between the calcium environment and the observed Ca K-pre-edge can be made. Further, it is demonstrated that the Ca site can serve as a reporter for the changes that occur at the Mn sites. The potential for future applications to the OEC are highlighted.

EXPERIMENTAL SECTION

Ca K-edge XAS data was collected on 13 model compounds consisting of both molecular and inorganic infinite lattices. A TD-DFT protocol was developed and correlated to the experimental data to help characterize the Ca K-pre-edge.

Compounds. *Inorganic Salts.* CaO (**6**[a]), $CaCO_3$ (**6**[b]), and $Ca(OH)_2$ (**6**[c]) were purchased at the highest available purity and used without further purification. CaO and $Ca(OH)_2$ were handled under anaerobic conditions.

Six and Seven Coordinate Ca Compounds. The ligand precursor H_3L, where L is a 1,3,5-triarylbenzene-based ligand, was prepared according to reported procedures.[52] The six coordinate $\{[LMn^{II}Mn^{III}{}_2O(OAc)_3]_2Ca\}^{2+}$ (**6**[d]) and seven coordinate molecular complexes $LMn^{IV}{}_3CaO_4(OAc)_3(THF)$ (**7**[e]), $LMn^{IV}{}_3CaO_4(OAc)_3$-(DMF) (**7**^{CUBox}), $[LMn^{IV}Mn^{III}{}_2CaO_2(OAc)_2(DME)(OTf)](OTf)_2$ (**7**^{NCox}), and $[LMn^{III}{}_3CaO_2(OAc)_2(DME)(OTf)](OTf)$ (**7**^{NCred}; Figure 1) were synthesized as previously described.[53−56] XAS samples of $[LMn^{IV}{}_2Mn^{III}CaO_4(OAc)_3(DMF)]^-$ (**7**^{CUBred}) were prepared by the addition of 1 equiv of cobaltocene to a solution of **7**^{CUBox} in DMF. The reaction mixture was then transferred to 40 μL XAS liquid sample holders and frozen within 5 min of reductant addition. Attempts to isolate **7**^{CUBred} as a solid in analytically pure form have been unsuccessful to date.

Eight Coordinate Ca Compounds. The ligand precursors H_3tpaa (6,6′,6″-nitrilotris(methylene)tripicolinic acid) and H_2dpaea (*N*,*N*-bis[6-carboxypyridin-2-yl)methyl]ethylamine) and compound $[Ca(dpaea)(H_2O)(MeOH)]_2$ (**8**[g]) were prepared according to reported procedures.[57−59] All other starting materials including the H_2bzida ligand (N-benzyliminodiacetic acid) were commercially available. The elemental analyses were carried out with a C, H, N analyzer (SCA, CNRS).

*Synthesis of [Ca(Htpaa)(H$_2$O)] (**8**^{f}).* An aqueous solution of KOH (0.1 M) was added to a suspension of H_3tpaa (40.0 mg, 94.70 μmol) in water (5 mL) until pH ∼5 was reached, yielding a colorless solution. Solid $CaCl_2{\cdot}2H_2O$ (14.0 mg, 95.23 μmol) was added to the resulting colorless solution, and after a few minutes of stirring, a white precipitate was formed. After stirring the mixture for 15 min, precipitation was completed by cooling the mixture to 4 °C for 12 h. The white powder was filtered off, washed with H_2O (2 mL), dried under a vacuum, and collected (yield, 20.0 mg, 37%). Anal. Calcd for $C_{21}H_{18}CaN_4O_7{\cdot}H_2O{\cdot}KCl$ (571.03): C, 44.17; H, 3.53; N, 9.81. Found: C, 44.32; H, 3.50; N, 9.68. This can be cocrystallized with the reported trinuclear compound $[\{Ca(tpaa)(OH_2)\}_2\{Ca(OH_2)_4\}]$ by slow evaporation of an aqueous solution of $tpaa^{3-}$ (pH 8), in the presence of 1 equiv of $CaCl_2{\cdot}2H_2O$.[59] XAS data were obtained for powder samples at pH 5.

*Synthesis of [Mn$_2$(tpaa)$_2$Ca$_2$(OH$_2$)$_{12}$]$^{2+}$ (**8**^{h}).* An aqueous solution of KOH (0.1 M) was added to an H_3tpaa (40.0 mg, 94.70 μmol) suspension in water (10 mL) until pH ∼8 was reached, yielding a colorless solution. Solid $MnCl_2$ (13.3 mg, 105.7 μmol) and $CaCl_2{\cdot}2H_2O$ (10.0 mg, 68.0 μmol) were successively added. The resulting colorless solution was stirred for 1 min. X-ray suitable colorless single crystals of $[Mn_2(tpaa)_2Ca_2(OH_2)_{12}][Mn(tpaa)]_2{\cdot}25H_2O$ were obtained upon standing for 24 h. These were filtered, washed with cold water (1 mL), and air-dried for a few days (yield, 29.0 mg, 50%). Anal. Calcd for $C_{84}H_{84}N_{16}O_{36}Mn_4Ca_2{\cdot}13H_2O$ (2427.76): C, 41.56; H, 4.57; N, 9.23. Found: C, 41.58; H, 4.29; N, 9.18.

*Synthesis of [Ca$_2$(bzida)$_2$(OH$_2$)$_6$]$_n$ (**8**^{i}).* An aqueous solution of KOH (0.1 M) was added to a suspension of H_2bzida (62.0 mg, 277.7 μmol) in water (5 mL) until pH ∼9 was reached, yielding a colorless solution. Solid $Ca(O_3SCF_3)_2$ (97.0 mg, 286.8 μmol) was added, and the resulting colorless solution was stirred for 10 min. X-ray suitable colorless single crystals of **8**^{i} were obtained by slow evaporation of the solvent at 20 °C. These were filtered, washed with cold water (four drops), and dried on standing for a few days (yield, 33.0 mg, 36%). Anal. Calcd for $C_{22}H_{34}Ca_2N_2O_{14}{\cdot}0.1C_{11}H_{13}NO_4$ (652.99): C, 42.49; H, 5.45; N, 4.50. Found: C, 42.45; H, 5.38; N, 4.73.

X-ray Structure Determination. Single-crystal diffraction data were taken using an Oxford-Diffraction XCalibur S Kappa geometry diffractometer (Mo Kα radiation, graphite monochromator, λ 0.71073 Å). An absorption correction was applied, using the ABSPACK Oxford-diffraction program with transmission factors in the 0.674−0.898 range.[60] The molecular structure was solved by direct methods and refined on F^2 by full matrix least-squares techniques using the SHELXTL package.[61] All non-hydrogen atoms were refined anisotropically, and hydrogen atoms were found by Fourier transformation and refined with individual isotropic displacement parameters. CCDC 995926, CCDC 995927, and CCDC 995923 contain the supplementary crystallographic data for **8**^{f}, **8**^{h}, and **8**^{i}, respectively. A summary of X-ray data collection and structure refinement for **8**^{i} is reported in Supporting Information Table S1.1. Selected bond distances and angles are provided in Table S1.2. The X-ray structure of **8**^{i}, together with the CIF file, is provided as Supporting Information. The structural description of the complexes **8**^{f} and **8**^{h} will be reported elsewhere.

XAS Data Collection and Sample Preparation. Solid samples were diluted in boron nitride and mounted on Ca-free polycarbonate holders. Air-sensitive and hygroscopic samples were prepared under anaerobic conditions. X-ray absorption spectroscopy (XAS) data on the seven coordinate calcium species (**7**^{NCox}, **7**^{NCred}, **7**^{CUBox}, **7**^{CUBred}, **7**^{e}) and on the six coordinate calcium complex **6**^{d} were measured at the Stanford Synchrotron Radiation Lightsource (3-GeV ring) beamline 4−3 equipped with a Si(111) double-crystal monochromator. A four-element silicon drift detector (Vortex-ME4, Hitachi) was used to collect the data as fluorescence excitation spectra. Samples were maintained at a temperature of ∼30 K with a liquid He cryostream (Oxford) to minimize radiation damage. Ca K-edge data were monitored throughout the course of data collection to ensure that no X-ray induced damage occurred. Further, to test for nonlocal damage, the Mn K-edge was monitored before and after collection of Ca XAS data on each sample.

All other data were collected at beamline A1 (DORIS light source at DESY, 4.5 GeV ring) equipped with a Si(111) double crystal monochromator and a vacuum sample chamber. Solid samples were diluted in boron nitride and finely dispersed on Kapton tape (K104 PSA polyimide film with silicone adhesive). Data were collected in fluorescence mode using a PIPS-diode detector. Samples were monitored for radiation damage throughout the course of data collection.

XAS Data Processing. Spectra were calibrated to the maxima of the rising edge feature in calcium acetate monohydrate set at 4050.0 eV. The Athena software program, using the AUTOBK algorithm, was used for data reduction and normalization.[62] A linear pre-edge function and a quadratic polynomial for the postedge were used for background subtraction, followed by normalization of the edge jump. In order to extract intensities and energy positions of pre-edge features, the Ca K-edges were fit with Gaussian−Lorentzian sum peaks and a cumulative Gaussian−Lorentzian function for the edge jump. The intensity of the features corresponds to the integrated area under the peaks. The software package PeakFit v 4.12 was used for the fitting.

dx.doi.org/10.1021/ic501991e | Inorg. Chem. 2015, 54, 1283−1292

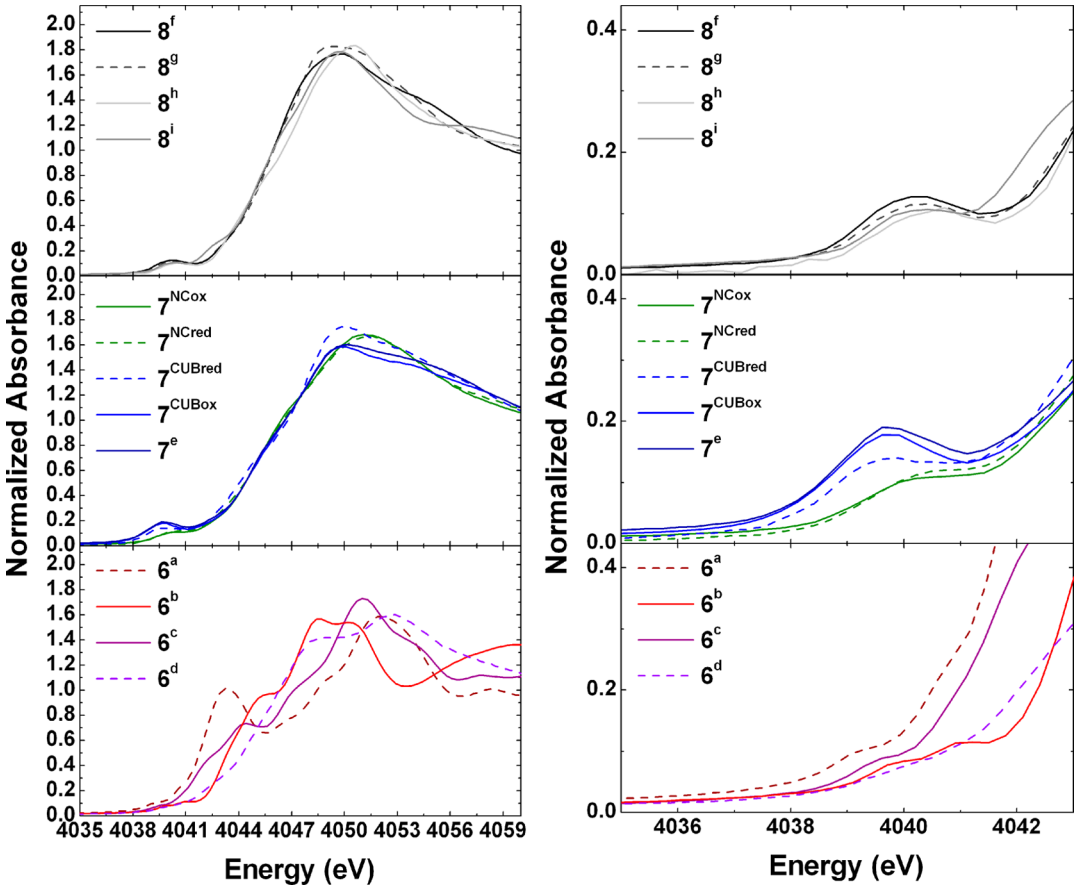

Figure 2. X-ray absorption spectra at the Ca K-edge of six (bottom), seven (middle), and eight (top) coordinate Ca^{2+} species: Full rising edge of the spectra (left) and the pre-edge region (right).

Computational Details. All DFT calculations were carried out using the ORCA program.[63] In general, for molecular complexes, crystal structures with the full ligands were used to generate the starting coordinates for geometry optimization calculations. Geometry optimizations were carried out with the spin-unrestricted Kohn−Sham method using the TPSS functional[64] and a def2-TZVP basis set with a def2-TZVP/J auxiliary basis set,[65,66] as well as a DFT-D3BJ dispersion correction.[67,68] A dense integration grid (ORCA Grid4 = Lebedev 302 points) was used for all the atoms except Ca and Mn where a Grid6 (Lebedev 590 points) was applied. The geometry-optimized structures were later used for the Ca K-pre-edge XAS spectra calculations. There are three exceptions to the approach outlined above. The $\mathbf{8}^{i}$ polymer was truncated to a $[Ca_2(bzida)_2(OH_2)_6]$ repeating unit, before geometry optimization, as described in Supporting Information S2. Additionally, the model for the $\mathbf{7}^{CUBred}$ complex was based on the crystal structure of the previously published Sc analog.[55] The Sc atom was replaced with Ca, and the structure was optimized, while maintaining Mn-ligand bond distances of the original complex. This was in lieu of a crystal structure for $\mathbf{7}^{CUBred}$. Lastly, the model for the XAS spectral calculation of $\mathbf{6}^{d}$ was truncated after geometry optimization to encompass the Ca center and acetate ligands, with proton capped oxygens instead of Mn−O bonds (Supporting Information S2). The truncation of the model was needed due to the large size of the molecular complex.

In models for CaO ($\mathbf{6}^{a}$), $CaCO_3$ ($\mathbf{6}^{b}$), and $Ca(OH)_2$ ($\mathbf{6}^{c}$), inorganic lattices were built using the effective core potential embedding approach. In the most popular variant of this approach,[69−71] the quantum cluster (QC) is embedded in an extended point charge field (PC). Furthermore, in order to avoid electron attraction or electron−flow from the quantum cluster region toward the positive charges at the PC region, a third boundary region (BR) is introduced between QC and PC, which is constructed from repulsive capped effective core potentials (c-ECPs). In all the cases, the QC is constructed around the central calcium center spanning a 5 Å radius region around it. Additionally the BR is extended to about 8 Å from the calcium center. The respective atom centers were exchanged by capped effective core potentials (with ECP basis sets SD(10,MWB)[72] for Ca and SD(2,MWB)[73] for O and C). Finally, the PC region follows the BR, extending 15 Å from the central calcium. The charges for the three regions were distributed such that the net charge for the model is zero and the total charges for the border and point charge region taken together offset the charge on the quantum cluster region.

Calcium K-edge XAS spectra were calculated with a TD-DFT approach[39,40] employing the Tamm−Dancoff approximation as implemented in ORCA.[74] Spin unrestricted calculations were carried out using a large integration grid (Grid5 = Lebedev 434 points) and the BHLYP functional.[75] As previous studies have shown, the choice of functional can impact the calculated XAS spectra, we also carried out a detailed study on the functional dependence. The BHLYP functional was found to offer the best results in terms of resolving the pre-edge consistent with previously reported studies (Supporting Information S3).[41,42,44,76,77] The RIJCOSX approximation was implemented to help reduce the computational cost of the TD-DFT calculations.[78] For these calculations, the def2-TZVP basis set with a def2-QZVPP/JK auxiliary basis set was used on all atoms except calcium where a def2-QZVP basis set was employed.[66] In order to ensure saturation of the particle/hole transitions spanning the pre-edge and near edge region of the Ca K-edge spectra, the basis of ∼20 nonrelativistic roots was calculated. Moreover the calculated intensities include electric dipole, magnetic dipole, and quadrupole contributions.[40]

RESULTS

Model Complexes. Ca K-edge data were obtained for a series of 13 inorganic lattice and molecular complexes (Figure 1

dx.doi.org/10.1021/ic501991e | Inorg. Chem. 2015, 54, 1283−1292

and Table 1). The six coordinate complexes consist of pseudo-octahedral species with increasing complexity of the oxygen-based ligands. CaO ($\mathbf{6}^{a}$) can be considered octahedral, followed by $\mathbf{6}^{d}$, which has only small distortions from octahedral symmetry and $CaCO_3$ ($\mathbf{6}^{b}$), which has local D_{4h} symmetry. Finally, $Ca(OH)_2$ ($\mathbf{6}^{c}$) has an approximate D_{2h} arrangement. Four seven-coordinate complexes, which mimic the Mn_4O_5Ca cluster motifs in the OEC, were investigated. These complexes can be grouped as having a "cubane-like" structure (7^{CUBox}, 7^{e}) and a "noncubane-like" structure (7^{NCox}) depending on the arrangement of the metal-oxo atoms. Furthermore, one-electron oxidized and reduced pairs of these complexes were investigated. The cubane-like complexes can be best described as having C_{3v} symmetry at the calcium center, while the noncubanes favor a C_{2v} symmetry. To offer a full range of accessible coordination geometries, eight coordinate calcium species ($\mathbf{8}^{f}$, $\mathbf{8}^{g}$, $\mathbf{8}^{h}$, and $\mathbf{8}^{i}$) having a mixture of amine, carboxylate, and water ligands were also investigated. Calcium geometries for $\mathbf{8}^{f}$ and $\mathbf{8}^{g}$ are best described as trigonal dodecahedron (D_{2d}), while $\mathbf{8}^{h}$ and $\mathbf{8}^{i}$ are more pseudosquare antiprismatic having a symmetry best characterized as intermediary between D_{4d} and D_{2d}. The symmetries around the Ca centers are approximated to the first coordination sphere ligand atoms.

X-ray Absorption Spectroscopy. Figure 2 shows the Ca K-edge spectra for all investigated compounds. In the case of molecular complexes, the rising edges are similar, and the largest variations occur in the pre-edge region. However, in the inorganic infinite lattice series, the rising edge is dominated by a convolution of multiple scattering and absorption processes resulting in significant variability. Such features have previously been reproduced using multiple scattering theory; however this approach fails to capture the pre-edge region, which is an important probe of coordination environment at the absorbing center.[79,80] For these reasons, we focus on the pre-edge region between ~4038 eV and ~4042 eV (Figure 2; right). The low intensities of the features compared to the rising edge are reminiscent of the 1s → 3d dipole forbidden transitions of pre-edges in transition metals (TM) and have previously been assigned as such based largely on empirical considerations[21−29,31,81,82] and, more recently, based on a density of states analysis of CaS infinite lattices.[80]

Six coordinate species are distinguished from seven and eight coordinate centers by the presence of two pre-edge features split by ~1 eV and a lower intensity pre-edge. The pre-edge maxima for six coordinate centers occur at ~4039.5 eV and ~4040.6 eV, thus spanning the energies of the maxima for seven and eight coordinate complexes (Figures 2 and 3). The most intense pre-edges occur in the seven coordinate "cubane-like" structures at ~4039.75 eV. Furthermore, a one electron chemical reduction of the 7^{CUBox} "cubane-like" complex $[Mn^{IV}_3CaO_4]$ to yield 7^{CUBred} $[Mn^{IV}_2Mn^{III}CaO_4]$ results in a ~16 ± 3% lower intensity pre-edge. This is not observed upon one electron chemical reduction of the "noncubane" 7^{NCox} to yield 7^{NCred}, both of which have pre-edges centered around ~4040.17 eV, similar in intensity and energy to eight coordinate calcium complexes.

As K-edge XAS transition intensities are predominantly dipole dependent (1s → *n*p), the variation in pre-edge intensities can in part be rationalized using symmetry arguments. Six coordinate pseudo-octahedral complexes are centro-symmetric with little or no p−d mixing, resulting in low intensity dipole forbidden (but quadrupole) 1s → 3d transitions into the t_{2g} and e_g orbitals. In the seven and eight coordinate complexes under study, this centro-symmetry is broken, p−d mixing becomes favored, and an increase in intensity occurs due to an increase in p-character mixing in the d manifold. The pre-edges are most intense for the cubane-like structures because they have pseudo C_{3v} symmetry and p mixing is symmetry allowed with all five d orbitals. Furthermore, the increase in the average pre-edge energy upon increasing the coordination number is most likely attributed to destabilization of the d manifold upon increasing the number of ligands. Similar effects on the pre-edge energies of the first row TM have previously been reported.[43,83]

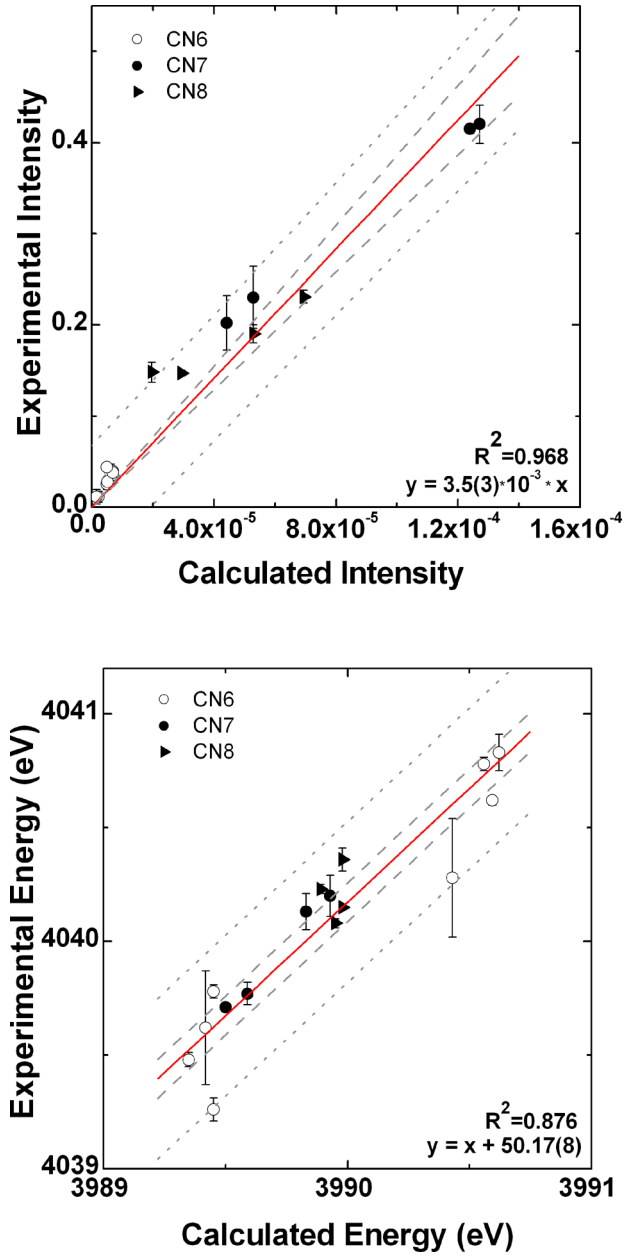

Figure 3. Correlation between experimental and calculated Ca K-edge XAS spectra. Intensity correlation (top); energy correlation (bottom). Best fit line (red), 95% confidence interval (dashed gray), 95% prediction band (dotted gray).

Calibration of Calculated Ca K-pre-edge XAS Spectra. In order to obtain a deeper understanding of the observed modulations in Ca K-pre-edge intensities and energies, a TD-

dx.doi.org/10.1021/ic501991e | Inorg. Chem. 2015, 54, 1283−1292

DFT approach was developed and calibrated to the experimental spectra. Owing to the limitations of DFT to accurately estimate the energies of the transition probabilities dominating the Ca K-pre-edge spectra, an empirical, element specific shift should be determined. In fact, the calculated absolute transition energies carry large but highly systematic errors that arise from shortcomings of the density functionals in the core region, limitations of the one-particle basis set, and shortcomings in the accurate modeling of spin-free relativistic effects. Given their highly systematic nature, all of these factors can (for a given basis set and density functional) be taken into account by introducing an element-dependent shift.[39,42,71,84−87] In fact, it has been shown that a simple linear regression is sufficient to establish predictive accuracy in the calculated transition energies for any given element. This calibration needs to be carried out with respect to a test set of well−known systems and has already been reported for metal and ligand K-edges in the framework of scalar relativistic DFT methodology.[39,42,84,85] The calibration of the Ca K-pre-edge spectra was performed for a series of 12 structurally characterized compounds. In all cases, good agreement between the calculated versus experimental pre-edge intensities and energies was observed (Figure 3, Table 1). The intensity correlation resulted in a linear relationship with an R^2 value of 0.968, while the energy correlation is also linear with an R^2 value of 0.876. Deviations may be attributed to errors intrinsic to data processing (Figure 3) and limitations of the theoretical models. For instance, while they are likely to be small,[88] possible vibronic contributions are not accounted for. Similarly, complexes of intermediate symmetry such as the eight coordinate D_{2d}/D_{4d} complex $\mathbf{8}^{h}$ may have a geometry optimized structure which does not fully capture the interplay between the limiting symmetries again causing deviations in calculated values from experiment. However, both the intensity and energy correlation values for goodness of fit are consistent with those of previously reported TD-DFT calculated XAS spectra and accurately predict the experimental trends observed as illustrated below.[41,42] From the calibration fits, the energy shift to be applied to the calculated transition energies was found to be 50.17 ± 0.08 eV, with an intensity normalization factor of 3500 ± 300.

DISCUSSION

Pre-edges of Ca K-edge XAS Spectra. Figure 4 shows an overlay of representative experimental Ca K-pre-edges, their corresponding fits, and the TD-DFT calculated transitions. Difference density maps were used to visualize the transitions in terms of a molecular orbital picture (Figure 5). The maps consist of a difference in electron density between the excited state and ground state and shows the shift in electron density due to the excitation.[89] As the Ca 1s orbital is highly localized and compact, the difference density map will be dominated by the contribution from the acceptor orbital.[89] From this analysis, it is evident that the Ca K-pre-edge consists of 1s → d excitations (Figures 4 and 5). In contrast to the first transition series, one generally does not consider a dominant 3d contribution to bonding in Ca. Nevertheless, the 3d orbitals are unoccupied and thus have XAS transitions, which may include both quadrupole (1s → 3d) and dipole allowed (1s → 3d + *n*p) transitions. It is the dipole allowed contribution that is responsible for the increase in pre-edge intensities over the present series.

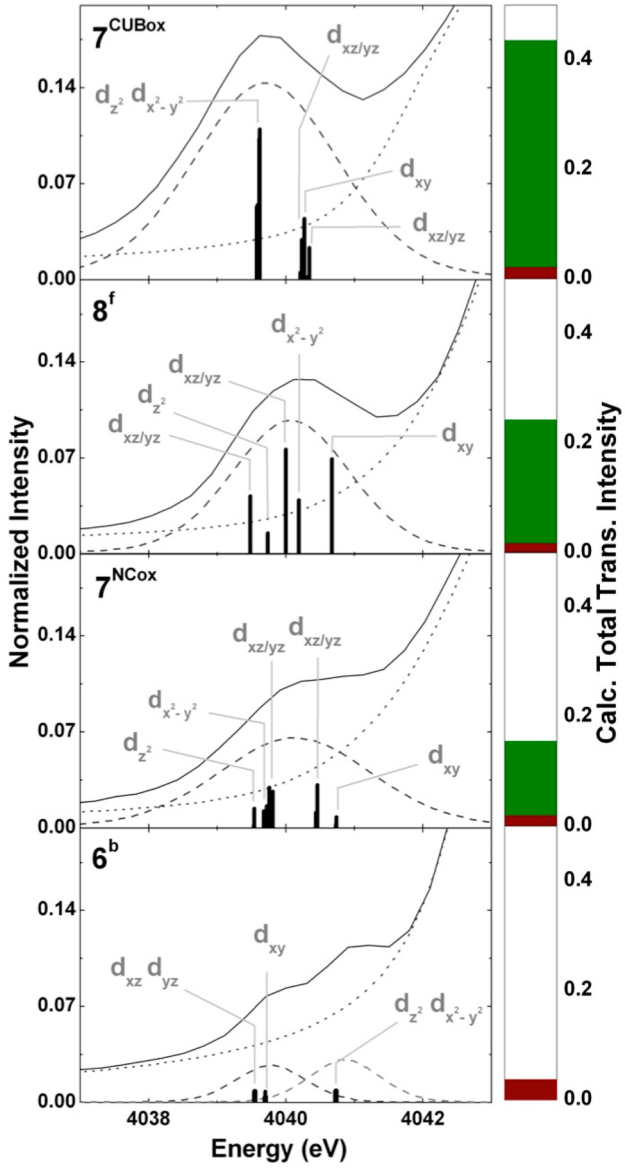

Figure 4. Pre-edges of Ca K-edge with their associated TD-DFT transitions and acceptor orbital assignment. From top to bottom: $\mathbf{7}^{CUBox}$, $\mathbf{8}^{f}$, $\mathbf{7}^{NCox}$, $\mathbf{6}^{b}$. (Left) Experimental spectra (black). Spectral fitting: rising edge (dotted lines), pre-edges (dashed lines). Calculated transition intensities (black bars). (Right) Breakdown of contributions to the total calculated transition intensities in terms of total dipole (green) and quadrupole (red) transition intensities, summed over the whole pre-edge. The calculated transition energies were shifted by 50.17 eV, and intensities were multiplied by a factor of 3500.

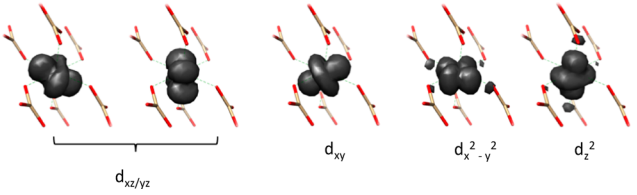

Figure 5. Difference density maps for 1s → 3d transitions in $\mathbf{6}^{b}$.

At the six coordinate pseudo-octahedral limit (Figure 4, $\mathbf{6}^{b}$), the pre-edge consists of two small features due to quadrupole transitions. The calculated and experimental spectra both show a ∼1 eV split with transitions roughly grouped into the t_{2g} and

dx.doi.org/10.1021/ic501991e | Inorg. Chem. 2015, 54, 1283−1292

e_g set of acceptor orbitals. This is due to destabilization of the d_{z^2} and $d_{x^2-y^2}$ orbitals upon interaction with the ligands (Figure 5). For the seven and eight coordinate complexes, there is an increase in intensity concomitant with the presence of dipole character. In the seven coordinate noncubane complex (7^{NCox}), with an approximate C_{2v} local symmetry at Ca, p−d mixing is formally allowed for all of the d orbitals except d_{xy}, which has the lowest calculated intensity. On the other hand, in the pseudo D_{2d} eight coordinate complex 8^f, p−d mixing is lowest in the d_{z^2} and $d_{x^2-y^2}$ orbitals, consistent with expectations from group theory. The most intense transitions are seen in the "cubane-like" seven coordinate 7^{CUBox} species, where the calcium center has a C_{3v} local symmetry that favors p−d mixing in all the d orbitals.

Model of p-Character Contributions. An *in silico* study of a hexa-aqua calcium complex, $[Ca(H_2O)_6]^{2+}$, was carried out in order to further understand the nature of p−d mixing responsible for intensity variations at the Ca K-pre-edge. A C_{4v} distortion was applied to a model octahedral $[Ca(H_2O)_6]^{2+}$ complex, with initial Ca−OH_2 distances of 2.4 Å, by varying the distance of one of the Ca−OH_2 axial bonds (Figure 6). Both

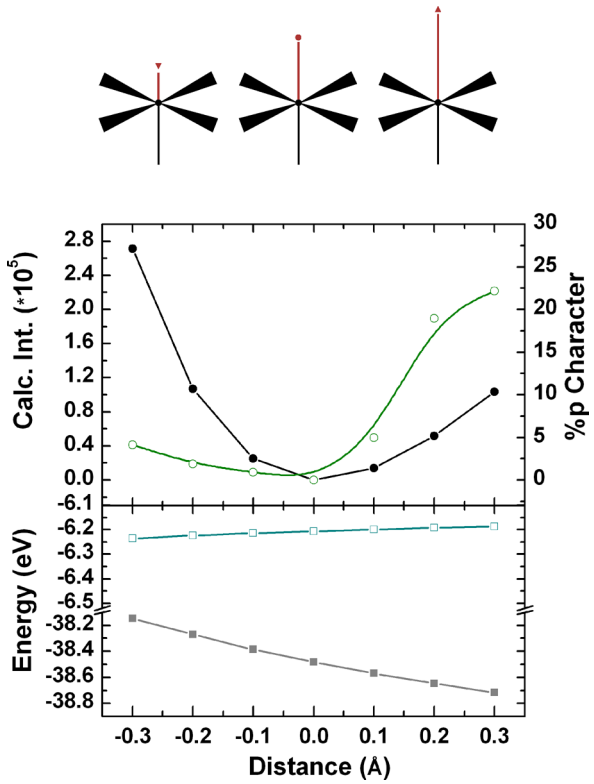

Figure 6. Effect of distortion from O_h to C_{4v} on $[Ca(H_2O)_6]^{2+}$. Symmetry lowering is achieved through compression or elongation of one axial Ca−OH_2 bond. (Top) Variation in pre-edge intensity (black) and p-character (green); (bottom) variation in 3p (gray) and 4p (cyan) orbital energies.

compression and elongation of the Ca−OH_2 axial bond are expected to enhance p−d mixing, through symmetry lowering and thus increase the pre-edge intensity. When the calculated intensities for all transitions in the pre-edge region are summed (black line, Figure 6), one observes that the maximum pre-edge intensity occurs upon the greatest compression or greatest elongation of the Ca−OH_2 bond. The calculated intensity is somewhat more enhanced for a compression of the Ca−OH_2 bond rather than an elongation, which may be in part explained by covalency arguments, as has been previously discussed.[90] However, if one sums the Ca p-character contributing to all acceptor molecular orbitals over the pre-edge region (green line, Figure 6), one finds that the percent p-character does not directly correlate with the intensity increase, as one might naively expect. This can be rationalized in terms of the origins of the p-character. Depending on the length of the Ca−ligand bond, in principle, both 3p and 4p orbitals can contribute, with 3p orbitals having larger contributions at shorter distances. It is important to recognize, however, that the 3p and 4p orbitals will have different intrinsic dipole moment integrals. A 1s → 3p dipole transition is expected to be significantly more intense than a 1s → 4p transition, as the 3p orbitals have far more contracted radial functions, resulting in a larger intrinsic transition dipole moment integral.[91,92]

It is then reasonable to discuss the changes in intensity as coming from p−d mixing with the p-character due to a combination of 3p and higher energy *n*p orbitals. Based on this hypothetical series, it is predicted that as the axial Ca-aqua bond distance is compressed, the 3p and 4p orbitals are closer in energy, and when the bond is elongated, their energies become more separated, with the 3p orbitals being largely responsible for the energy difference (Figure 6, bottom). As the 3p and higher *n*p orbitals become energetically closer, more 3p mixing into these orbitals is possible. Consequently as 3p mixing increases, less total p character is required for an increase in pre-edge intensity (Figure 6, top).

Ca K-edge XAS of PSII OEC Mimics. Thus far, the current study has shown a correlation between Ca K-pre-edges and Ca coordination geometry by comparing structurally characterized complexes with their experimental spectra. It is important, however, to be able to deduce structure−function relationships from experimental spectra even in the absence of *a priori* structural information. Compounds 7^e and 7^{CUBox} together with its one electron reduced analog 7^{CUBred} are good structural references for the Mn_3O_4Ca "cubane-like" part of the core of the OEC cluster.[53−55] These models offer an ideal test set for exploring the correlations between spectroscopic characteristics and geometric and electronic structures with relevance to the heterometallic cluster of the OEC. Cyclic voltammetry studies show that the one electron Mn centered reduction of 7^{CUBox} ($Mn^{IV}{}_3O_4Ca$) to 7^{CUBred} ($Mn^{III}Mn^{IV}{}_2O_4Ca$) occurs as a quasireversible wave at −890 mV versus ferrocene/ferrocenium in DMF.[54] However, while the structure 7^{CUBox} was characterized via crystallography, the structure for 7^{CUBred} was not. Therefore, a model was inferred for 7^{CUBred} based on the previously published analog, containing a Sc center instead of Ca.[55] Calculating the XAS spectrum, and comparing it to the experimentally determined 7^{CUBred} spectrum, supports this model's validity and demonstrates the ability of Ca K-edge XAS to provide structural information.

Experimentally, the 7^{CUBox} "cubane-like" complex has a distinct pre-edge signature at the Ca K-edge. A one electron chemical reduction leading to the 7^{CUBred} species results in a Ca K-edge spectrum with a ∼16 ± 3% lower pre-edge intensity (Table 1, Figure 7). A similar change in intensity is not observed in the noncubane complexes 7^{NCox} and 7^{NCred}, which have similar pre-edge intensities. This implies that factors other than electronegativity are the driving force for the changes in intensity. Complex 7^{CUBox} has a favorable geometry in terms of p−d mixing; however this is expected to change upon one electron reduction. Indeed, a Jahn−Teller like distortion (JT) is

dx.doi.org/10.1021/ic501991e | Inorg. Chem. 2015, 54, 1283−1292

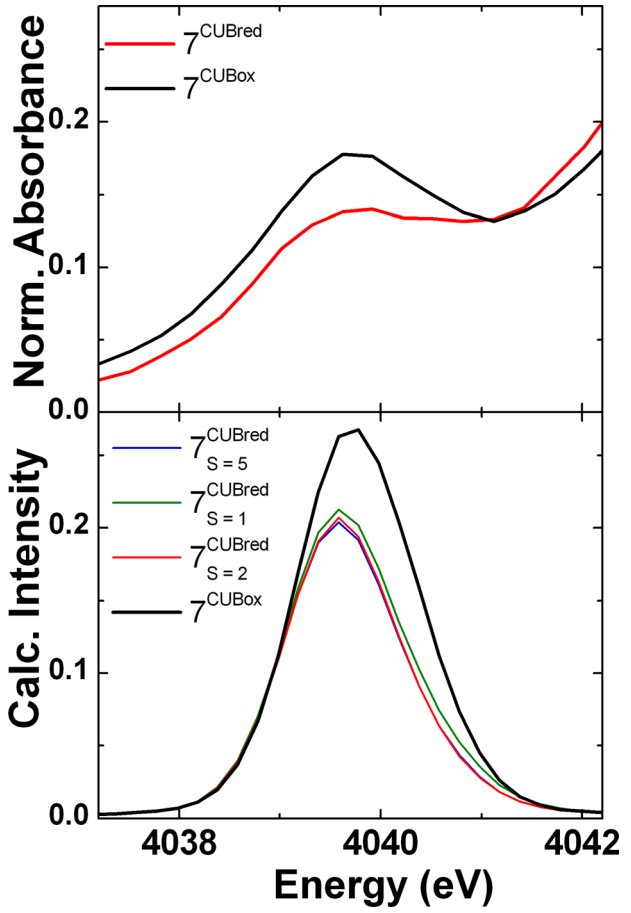

Figure 7. Experimental and calculated Ca K-pre-edge for 7^{CUBox} and 7^{CUBred}. Experimental spectra (top). Calculated spectra for 7^{CUBred} and 7^{CUBox} (bottom). Calculated pre-edge transitions were approximated as Gaussian–Lorentzian sum peaks (width 1.2 eV, shape 75% Gaussian). A 50.17 eV energy shift was applied, and intensities were multiplied by 3500 units.

predicted to occur at the Mn(III) center in the 7^{CUBred} model, resulting in subtle changes in both Ca bond distances and bond angles. The result is a calculated Ca K-pre-edge with a ~23% lower intensity in the reduced species 7^{CUBred} than in its oxidized counterpart (7^{CUBox}; Figure 7). Furthermore, the effect of total spin at the Mn centers on the calculated Ca K-pre-edge was explored. The XAS spectra for a high-spin (S = 5) system, as well as Mn(III)–Mn(IV) (S = 1) and Mn(IV)–Mn(IV) (S = 2) antiferromagnetically coupled systems were calculated, and the spin state was found not to have any significant impact on the Ca K-pre-edge (Figure 7). Similarly, previous work by Pantazis et al. used an *in silico* truncated model of 7^{CUBox} to investigate the possible reduction of each of the Mn(IV) centers to Mn(III) and the resulting preferred JT distortion.[93] Three lowest energy structural models for the reduced 7^{CUBox} were proposed, of which two were high-spin (S = 5) and one was of intermediate spin (S = 2). Calculation of Ca K-edge spectra for these models all resulted in a ~25% decrease in intensity for the pre-edge, independent of spin state, comparable to the result from using the 7^{CUBred} model presented herein (Supporting Information Figure S5).

CONCLUSIONS

A series of six, seven, and eight coordinate calcium compounds were systematically investigated using Ca K-edge XAS. The spectra of six coordinate complexes are distinguished by a low intensity pre-edge split by ~1 eV corresponding to excitations from the 1s orbital to the t_{2g} and e_g set of 3d orbitals. Seven and eight coordinate species consist of a single well-resolved 1s → 3d feature in the pre-edge with seven coordinate Mn_3O_4Ca "cubane-like" (7^{CUBox}, 7^{e}) clusters having the most intense pre-edges.

A TD-DFT based protocol was developed to calculate and analyze the Ca K-pre-edges. It was found that the determining factor for the pre-edge is the calcium coordination number and geometry. The intensities of the transitions are dependent on p–d mixing, which is least favored in six coordinate centrosymmetric species and becomes more favored as the symmetry is lowered in seven and eight coordinate complexes. At the C_{3v} limit, which best characterizes the "cubane-like" complexes, the highest pre-edge intensities are observed. The distribution of the transition energies correlates with an energetically destabilizing interaction with the ligands, where 3d orbitals interacting with the ligands are higher in energy.

Furthermore, we have investigated the potential applicability of Ca K-edge XAS to probe changes in the Mn_4O_5Ca cluster of the OEC as it progresses through the Kok cycle. Such investigations could provide important complementary information to existing Mn XAS data, while offering a more streamlined analysis due to the presence of only one Ca in the cluster, as opposed to four Mn ions. It is already evident that Ca XAS is sensitive to the ligand coordination environment directly surrounding the Ca center in terms of coordination number and ligand geometry. Since calcium is proposed to play a direct role in the catalytic cycle by binding one substrate water molecule, Ca K-edge XAS could potentially make an important contribution in further understanding the mechanism of water oxidation. However, the question arises if XAS at the Ca center of the OEC is sensitive to "global changes" of the cluster. Using the OEC closed cubane cluster mimics, 7^{CUBox} and its one electron reduced analog 7^{CUBred}, the sensitivity of Ca XAS to a one electron reduction at one of the three Mn centers was investigated. It was found that reduction of one Mn(IV) to Mn(III) produces a JT distortion at the Mn, which can be detected through changes in the Ca K-pre-edge XAS data. These studies thus establish Ca XAS as a potentially powerful probe for the understanding of the geometric and electronic structural changes that occur at the OEC. For example, Ca K-pre-edge XAS could be used to differentiate between the proposed OEC S_2 state conformations that consist of the "open-cubane" form with an EPR signal centered at g ~ 2.0 and a "closed-cubane" form with an EPR signal centered at g ~ 4.1.[10,94] The "closed-cubane" S_2 state model has a "cubane-like" Mn_3O_4Ca structural motif, analogous to the "cubane-like" model series presented herein, connected to the remaining "dangling" Mn by a Mn–O–Mn *oxo* bridge. The "open" conformation on the other hand has a structurally distorted cubane motif where the calcium forms an oxo bridge with the "dangling" Mn.[10,94] The current XAS study strongly suggests that there should be distinct differences in the Ca K-pre-edges of the two models, and therefore the application of these methods to the S states of the OEC are the subject of ongoing research in our laboratories.

ASSOCIATED CONTENT

Supporting Information

The Supporting Information includes a description of the X-ray structure of 8^{i} (section S1), a description of how the 8^{i} and 6^{d}

dx.doi.org/10.1021/ic501991e | Inorg. Chem. 2015, 54, 1283–1292

theoretical models were constructed (section S2), the functional correlation study (section S3), Ca K-edge calculated pre-edges and experimentally derived fitted pre-edges (section S4), the Ca K- pre-edge calculated XAS spectra of the Pantazis et al. truncated model of 7^{CUBred} (section S5), selected bond distances and XYZ coordinates of the geometry optimized models as well as the quantum clusters for the inorganic lattices (section S6), and the crystallographic information file for 8^{i}. This material is available free of charge via the Internet at http://pubs.acs.org.

AUTHOR INFORMATION

Corresponding Author

*E-mail: serena.debeer@cec.mpg.de.

Author Contributions

All authors have given approval to the final version of the manuscript.

Notes

The authors declare no competing financial interest.

ACKNOWLEDGMENTS

V.M.-D., D.M., V.K., and S.D. acknowledge the Max Planck Society for funding. S.D. acknowledges a Sloan Fellowship. B.G. thanks the "Université Joseph Fourier of Grenoble" for his Ph.D. grant. The Authors acknowledge support from ICMG FR 2067, COST CM1202 program (PERSPECT H2O), LABEX ARCANE (ANR-11-LABX-0003-01), the French National Research Agency (ANR-09-JCJC-0087 (MANGACOM), and ANR-13-BS07-0015-01 (MnCaOEC)) for financial support including M.G.'s and E.G.'s fellowships. We are grateful to the NIH (R01 GM102687A to T.A.); Dreyfus, Sloan, and Cottrell fellowships (T.A.); the NSF (GRFP to J.K. and E.T.); and Sandia National Laboratory (fellowship to E.T.) for funding. A portion of the XAS work was supported by NIH Grant F32GM100595 (R.T.), and by the Director of the Office of Basic Energy Science (OBES), Division of Chemical Sciences, Geosciences, and Biosciences, DOE, under contract DE-AC02-05CH11231 (J.Y). Use of the Stanford Synchrotron Radiation Lightsource, SLAC National Accelerator Laboratory, is supported by the U.S. Department of Energy, Office of Science, Office of Basic Energy Sciences under Contract No. DE-AC02-76SF00515. Parts of this research were carried out at the light source DORIS at DESY, a member of the Helmholtz Association (HGF). We would like to thank Dr. Edmund Welter for assistance in using beamline A.1.

REFERENCES

(1) Berridge, M. J.; Lipp, P.; Bootman, M. D. *Nat. Rev. Mol. Cell. Biol.* **2000**, *1*, 11−21.
(2) Brini, M.; Cali, T.; Ottolini, D.; Carafoli, E. *FEBS J.* **2013**, *280*, 5385−5397.
(3) Carafoli, E.; Santella, L.; Branca, D.; Brini, M. *Crit. Rev. Biochem. Mol.* **2001**, *36*, 107−260.
(4) Sorensen, A. B.; Sondergaard, M. T.; Overgaard, M. T. *FEBS J.* **2013**, *280*, 5511−5532.
(5) Arias-Moreno, X.; Abian, O.; Vega, S.; Sancho, J.; Velazquez-Campoy, A. *Curr. Protein Pept. Sci.* **2011**, *12*, 325−338.
(6) Campbell, R. L.; Davies, P. L. *Biochem. J.* **2012**, *447*, 335−351.
(7) Eijsink, V. G. H.; Matthews, B. W.; Vriend, G. *Protein Sci.* **2011**, *20*, 1346−1355.
(8) Becker, K.; Cormann, K. U.; Nowaczyk, M. M. *J. Photochem. Photobiol., B* **2011**, *104*, 204−211.
(9) Brudvig, G. W. *Philos. Trans. R. Soc., B* **2008**, *363*, 1211−1218.
(10) Cox, N.; Pantazis, D. A.; Neese, F.; Lubitz, W. *Acc. Chem. Res.* **2013**, *46*, 1588−1596.
(11) Yachandra, V. K.; Yano, J. *J. Photochem. Photobiol., B* **2011**, *104*, 51−59.
(12) Yusuf, N. N. A. N.; Kamarudin, S. K.; Yaakob, Z. *Biofuels, Bioprod. Biorefin.* **2012**, *6*, 319−334.
(13) Zhang, J.; Chen, S.; Yang, R.; Yan, Y. *Fuel* **2010**, *89*, 2939−2944.
(14) Kouzu, M.; Hidaka, J. *Fuel* **2012**, *93*, 1−12.
(15) Tao, Z.; Yang, Y.; Zhang, C.; Li, T.; Wang, J.; Wan, H.; Xiang, H.; Li, Y. *Catal. Comm.* **2006**, *7*, 1061−1066.
(16) Harder, S. *Chem. Rev.* **2010**, *110*, 3852−3876.
(17) Haven, T.; Kubik, G.; Haubenreisser, S.; Niggemann, M. *Angew. Chem., Int. Ed.* **2013**, *52*, 4016−4019.
(18) Jochmann, P.; Davin, J. P.; Spaniol, T. P.; Maron, L.; Okuda, J. *Angew. Chem., Int. Ed.* **2012**, *51*, 4452−4455.
(19) Liu, B.; Roisnel, T.; Carpentier, J. F.; Sarazin, Y. *Angew. Chem., Int. Ed.* **2012**, *51*, 4943−4946.
(20) Carpentier, J. F.; Sarazin, Y. In *Alkaline-Earth Metal Compounds: Oddities and Applications*; Harder, S., Ed.; Springer-Verlag Berlin: Berlin, 2013; Vol. *45*, pp 141−189.
(21) Eichert, D.; Salome, M.; Banu, M.; Susini, J.; Rey, C. *Spectrochim. Acta, Part B* **2005**, *60*, 850−858.
(22) Lam, R. S. K.; Charnock, J. M.; Lennie, A.; Meldrum, F. C. *CrystEngComm* **2007**, *9*, 1226−1236.
(23) Laurencin, D.; Almora-Barrios, N.; de Leeuw, N. H.; Gervais, C.; Bonhomme, C.; Mauri, F.; Chrzanowski, W.; Knowles, J. C.; Newport, R. J.; Wong, A.; Gan, Z.; Smith, M. E. *Biomaterials* **2011**, *32*, 1826−1837.
(24) Levi-Kalisman, Y.; Raz, S.; Weiner, S.; Addadi, L.; Sagi, I. *Adv. Funct. Mater.* **2002**, *12*, 43−48.
(25) Nguyen, C.; Ea, H. K.; Thiaudiere, D.; Reguer, S.; Hannouche, D.; Daudon, M.; Liote, F.; Bazin, D. *J. Synchrotron Radiat.* **2011**, *18*, 475−480.
(26) Politi, Y.; Levi-Kalisman, Y.; Raz, S.; Wilt, F.; Addadi, L.; Weiner, S.; Sagi, I. *Adv. Funct. Mater.* **2006**, *16*, 1289−1298.
(27) Veiga, J. P.; Figueiredo, M. O. *Appl. Phys. A: Mater. Sci. Process.* **2008**, *92*, 229−233.
(28) Fulton, J. L.; Heald, S. M.; Badyal, Y. S.; Simonson, J. M. *J. Phys. Chem. A* **2003**, *107*, 4688−4696.
(29) Kirkpatrick, R. J.; Brown, G. E.; Xu, N.; Cong, X. D. *Adv. Cem. Res.* **1997**, *9*, 31−36.
(30) RiggsGelasco, P. J.; Mei, R.; Ghanotakis, D. F.; Yocum, C. F.; PennerHahn, J. E. *J. Am. Chem. Soc.* **1996**, *118*, 2400−2410.
(31) Tongraar, A.; T-Thienprasert, J.; Rujirawat, S.; Limpijumnong, S. *Phys. Chem. Chem. Phys.* **2010**, *12*, 10876−10887.
(32) Loeb, K. E.; Zaleski, J. M.; Westre, T. E.; Guajardo, R. J.; Mascharak, P. K.; Hedman, B.; Hodgson, K. O.; Solomon, E. I. *J. Am. Chem. Soc.* **1995**, *117*, 4545−4561.
(33) Westre, T. E.; Loeb, K. E.; Zaleski, J. M.; Hedman, B.; Hodgson, K. O.; Solomon, E. I. *J. Am. Chem. Soc.* **1995**, *117*, 1309−1313.
(34) Loeb, K. E.; Westre, T. E.; Kappock, T. J.; Mitic, N.; Glasfeld, E.; Caradonna, J. P.; Hedman, B.; Hodgson, K. O.; Solomon, E. I. *J. Am. Chem. Soc.* **1997**, *119*, 1901−1915.
(35) Herbst, R. W.; Perovic, I.; Martin-Diaconescu, V.; O'Brien, K.; Chivers, P. T.; Pochapsky, S. S.; Pochapsky, T. C.; Maroney, M. J. *J. Am. Chem. Soc.* **2010**, *132*, 10338−10351.
(36) Banaszak, K.; Martin-Diaconescu, V.; Bellucci, M.; Zambelli, B.; Rypniewski, W.; Maroney, M. J.; Ciurli, S. *Biochem. J.* **2012**, *441*, 1017−1026.
(37) Martin-Diaconescu, V.; Bellucci, M.; Musiani, F.; Ciurli, S.; Maroney, M. J. *J. Biol. Inorg. Chem.* **2012**, *17*, 353−361.
(38) Zambelli, B.; Berardi, A.; Martin-Diaconescu, V.; Mazzei, L.; Musiani, F.; Maroney, M. J.; Ciurli, S. *J. Biol. Inorg. Chem.* **2014**, *19*, 319−334.
(39) DeBeer George, S.; Petrenko, T.; Neese, F. *Inorg. Chim. Acta* **2008**, *361*, 965−972.
(40) DeBeer George, S.; Petrenko, T.; Neese, F. *J. Phys. Chem. A* **2008**, *112*, 12936−12943.

(41) Lima, F. A.; Bjornsson, R.; Weyhermuller, T.; Chandrasekaran, P.; Glatzel, P.; Neese, F.; DeBeer, S. *Phys. Chem. Chem. Phys.* **2013**, *15*, 20911−20920.
(42) Roemelt, M.; Beckwith, M. A.; Duboc, C.; Collomb, M.-N.; Neese, F.; DeBeer, S. *Inorg. Chem.* **2012**, *51*, 680−687.
(43) Westre, T. E.; Kennepohl, P.; DeWitt, J. G.; Hedman, B.; Hodgson, K. O.; Solomon, E. I. *J. Am. Chem. Soc.* **1997**, *119*, 6297−6314.
(44) Atkins, A. J.; Jacob, C. R.; Bauer, M. *Chem.—Eur. J.* **2012**, *18*, 7021−7025.
(45) Bauer, M. *Phys. Chem. Chem. Phys.* **2014**, *16*, 13827−13837.
(46) Bordiga, S.; Bonino, F.; Damin, A.; Lamberti, C. *Phys. Chem. Chem. Phys.* **2007**, *9*, 4854−4878.
(47) Frank de, G.; György, V.; Pieter, G. *J. Phys.: Condens. Matter* **2009**, *21*, 104207.
(48) Mijovilovich, A.; Hayashi, H.; Kawamura, N.; Osawa, H.; Bruijnincx, P. C. A.; Klein Gebbink, R. J. M.; de Groot, F. M. F.; Weckhuysen, B. M. *Eur. J. Inorg. Chem.* **2012**, *2012*, 1589−1597.
(49) Swarbrick, J. C.; Kvashnin, Y.; Schulte, K.; Seenivasan, K.; Lamberti, C.; Glatzel, P. *Inorg. Chem.* **2010**, *49*, 8323−8332.
(50) Vankó, G.; Neisius, T.; Molnár, G.; Renz, F.; Kárpáti, S.; Shukla, A.; de Groot, F. M. F. *J. Phys. Chem. B* **2006**, *110*, 11647−11653.
(51) Umena, Y.; Kawakami, K.; Shen, J.-R.; Kamiya, N. *Nature* **2011**, *473*, 55−U65.
(52) Tsui, E. Y.; Day, M. W.; Agapie, T. *Angew. Chem., Int. Ed.* **2011**, *50*, 1668−1672.
(53) Kanady, J. S.; Mendoza-Cortes, J. L.; Tsui, E. Y.; Nielsen, R. J.; Goddard, W. A., III; Agapie, T. *J. Am. Chem. Soc.* **2013**, *135*, 1073−1082.
(54) Kanady, J. S.; Tsui, E. Y.; Day, M. W.; Agapie, T. *Science* **2011**, *333*, 733−736.
(55) Tsui, E. Y.; Agapie, T. *Proc. Natl. Acad. Sci. U.S.A.* **2013**, *110*, 10084−10088.
(56) Tsui, E. Y.; Tran, R.; Yano, J.; Agapie, T. *Nat. Chem.* **2013**, *5*, 293−299.
(57) Bretonniere, Y.; Mazzanti, M.; Pecaut, J.; Dunand, F. A.; Merbach, A. E. *Chem. Com.* **2001**, 621−622.
(58) Bretonnière, Y.; Mazzanti, M.; Pécaut, J.; Dunand, F. A.; Merbach, A. E. *Inorg. Chem.* **2001**, *40*, 6737−6745.
(59) Pellissier, A.; Bretonnière, Y.; Chatterton, N.; Pécaut, J.; Delangle, P.; Mazzanti, M. *Inorg. Chem.* **2007**, *46*, 3714−3725.
(60) *ABSPACK*; Oxford Diffraction Ltd: Abingdon, Oxfordshire, England, 2010.
(61) Sheldrick, G. M. *SHELXTL*, version 6.14; Bruker AXS Inc.: Madison, WI, 1997.
(62) Ravel, B.; Newville, M. *J. Synchrot. Radiat.* **2005**, *12*, 537−541.
(63) Neese, F. *Wiley Interdiscip. Rev.: Comput. Mol. Sci.* **2012**, *2*, 73−78.
(64) Tao, J.; Perdew, J. P.; Staroverov, V. N.; Scuseria, G. E. *Phys. Rev. Lett.* **2003**, *91*, 146401.
(65) Schäfer, A.; Horn, H.; Ahlrichs, R. *J. Chem. Phys.* **1992**, *97*, 2571−2577.
(66) Weigend, F.; Ahlrichs, R. *Phys. Chem. Chem. Phys.* **2005**, *7*, 3297−3305.
(67) Grimme, S.; Antony, J.; Ehrlich, S.; Krieg, H. *J. Chem. Phys.* **2010**, *132*, -.
(68) Grimme, S.; Ehrlich, S.; Goerigk, L. *J. Comput. Chem.* **2011**, *32*, 1456−1465.
(69) Staemmler, V. *The Cluster Approach for the Adsorption of Small Molecules on Oxide Surfaces - Theorectical Aspects of Transition Metal Catalysis*; Springer: Berlin/Heidelberg, 2005; Vol. *12*, pp 219−256.
(70) Maganas, D.; Roemelt, M.; Haevecker, M.; Trunschke, A.; Knop-Gericke, A.; Schloegl, R.; Neese, F. *Phys. Chem. Chem. Phys.* **2013**, *15*, 7260−7276.
(71) Maganas, D.; DeBeer, S.; Neese, F. *Inorg. Chem.* **2014**, *53*, 6374−6385.
(72) Kaupp, M.; Schleyer, P. v. R.; Stoll, H.; Preuss, H. *J. Chem. Phys.* **1991**, *94*, 1360−1366.
(73) Bergner, A.; Dolg, M.; Küchle, W.; Stoll, H.; Preuß, H. *Mol. Phys.* **1993**, *80*, 1431−1441.
(74) Hirata, S.; Head-Gordon, M. *Chem. Phys. Lett.* **1999**, *314*, 291−299.
(75) Becke, A. D. *J. Chem. Phys.* **1993**, *98*, 1372−1377.
(76) Atkins, A. J.; Bauer, M.; Jacob, C. R. *Phys. Chem. Chem. Phys.* **2013**, *15*, 8095−8105.
(77) Bernadotte, S.; Atkins, A. J.; Jacob, C. R. *J. Chem. Phys.* **2012**, *137*, 204106.
(78) Neese, F.; Wennmohs, F.; Hansen, A.; Becker, U. *Chem. Phys.* **2009**, *356*, 98−109.
(79) Rehr, J. J.; Ankudinov, A. L. *Coord. Chem. Rev.* **2005**, *249*, 131−140.
(80) Xu, W.; Liu, L. J.; Cui, M. Q.; Zheng, L.; Hu, Y. F.; Marcelli, A.; Wu, Z. Y. *J. Synchrotron Radiat.* **2013**, *20*, 110−115.
(81) Bianconi, A.; Doniach, S.; Lublin, D. *Chem. Phys. Lett.* **1978**, *59*, 121−124.
(82) Cormier, L.; Neuville, D. R. *Chem. Geol.* **2004**, *213*, 103−113.
(83) Yamamoto, T. *X Ray Spectrom.* **2008**, *37*, 572−584.
(84) DeBeer George, S.; Neese, F. *Inorg. Chem.* **2010**, *49*, 1849−1853.
(85) Lee, N.; Petrenko, T.; Bergmann, U.; Neese, F.; DeBeer, S. *J. Am. Chem. Soc.* **2010**, *132*, 9715−9727.
(86) Beckwith, M. A.; Roemelt, M.; Collomb, M.-N. L.; DuBoc, C.; Weng, T.-C.; Bergmann, U.; Glatzel, P.; Neese, F.; DeBeer, S. *Inorg. Chem.* **2011**, *50*, 8397−8409.
(87) Roemelt, M.; Maganas, D.; DeBeer, S.; Neese, F. *J. Chem. Phys.* **2013**, *138*, 204101.
(88) Hahn, J. E.; Scott, R. A.; Hodgson, K. O.; Doniach, S.; Desjardins, S. R.; Solomon, E. I. *Chem. Phys. Lett.* **1982**, *88*, 595−598.
(89) Krewald, V.; Lassalle-Kaiser, B.; Boron, T. T.; Pollock, C. J.; Kern, J.; Beckwith, M. A.; Yachandra, V. K.; Pecoraro, V. L.; Yano, J.; Neese, F.; DeBeer, S. *Inorg. Chem.* **2013**, *52*, 12904−12914.
(90) DeBeer George, S.; Brant, P.; Solomon, E. I. *J. Am. Chem. Soc.* **2005**, *127*, 667−674.
(91) Neese, F.; Hedman, B.; Hodgson, K. O.; Solomon, E. I. *Inorg. Chem.* **1999**, *38*, 4854−4860.
(92) Delgado-Jaime, M. U.; DeBeer, S.; Bauer, M. *Chem.—Eur. J.* **2013**, *19*, 15888−15897.
(93) Krewald, V.; Neese, F.; Pantazis, D. A. *J. Am. Chem. Soc.* **2013**, *135*, 5726−5739.
(94) Pantazis, D. A.; Ames, W.; Cox, N.; Lubitz, W.; Neese, F. *Angew. Chem., Int. Ed.* **2012**, *51*, 9935−9940.